

Supplementary information

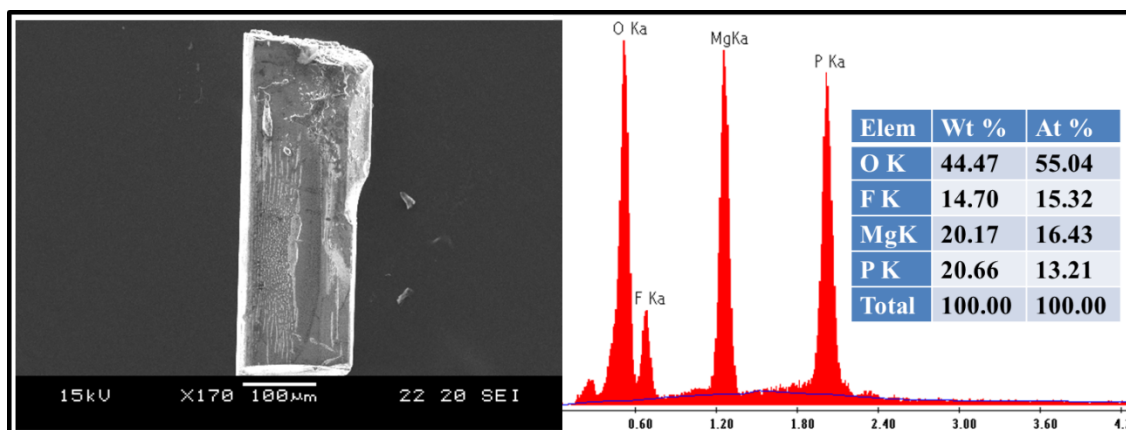


Figure S1. SEM images and EDX analyses of the $\text{Li}_2\text{Mg}[\text{PO}_4]\text{F}$ single crystal used for the data collection.

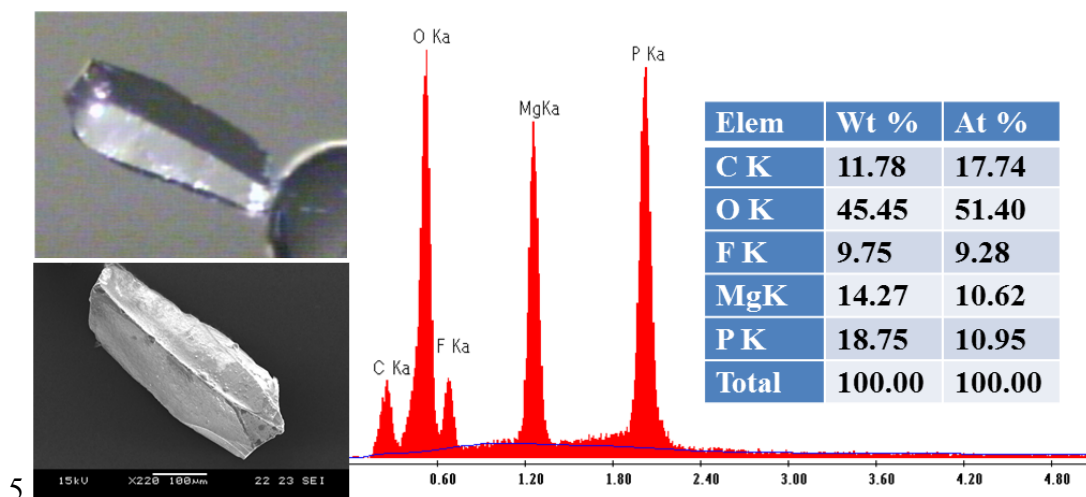


Figure S2. SEM and CCD images, and EDX analyses of the $\text{Li}_9\text{Mg}_3[\text{PO}_4]_4\text{F}_3$ single crystal used for the data collection.

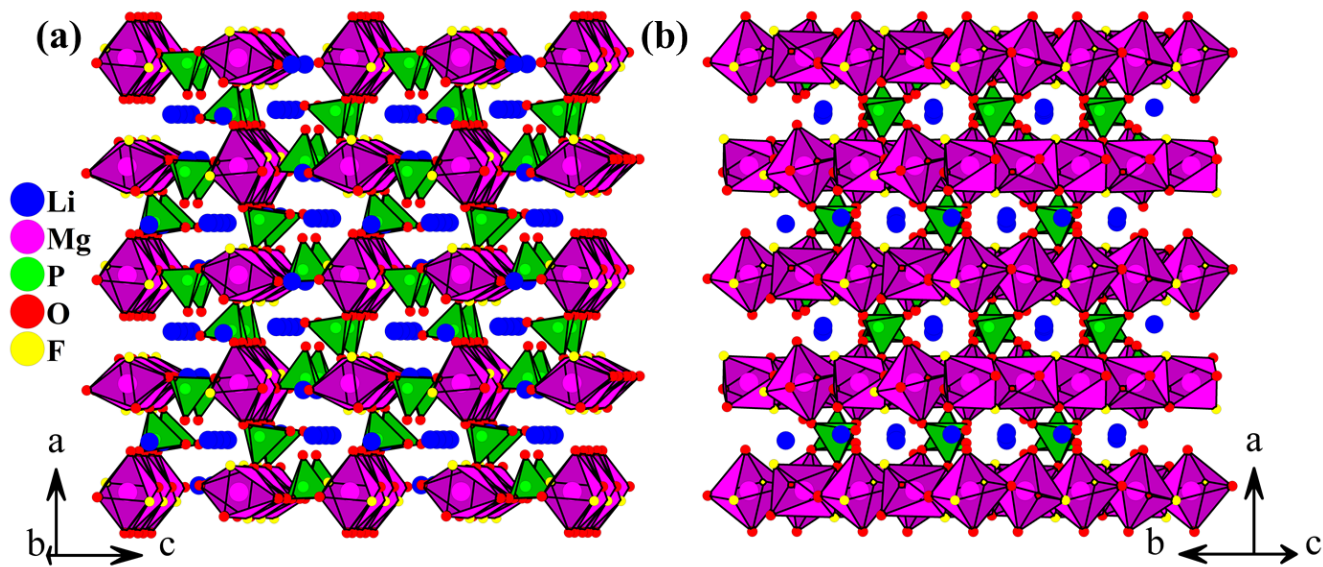


Figure S3. Views of the tunnels running along the [010] (a), and [011] directions (b).

$\text{Li}_2\text{Ni}[\text{PO}_4]\text{F}:\text{Li}_4\text{Ni}_2[\text{PO}_4]_2\text{F}_2$	Li1	Li2	Li3	Ni1	Ni2	P1	P2	O1	O2	O3	O4	O5	O6	F1	F2
<i>Pmma</i> (no. 62)	8d	4c	4c	4a	4b	4c	4c	8d	4c	4c	4c	4c	8d	4c	4c
$a = 10.4730 \text{ \AA}$	0.240	0.271	0.027	0	0	0.0236	0.2432	0.1891	0.2184	0.1694	0.3890	0.4739	0.0320	0.1272	0.4503
$b = 6.2887 \text{ \AA}$	0.012	1/4	1/4	0	0	1/4	1/4	0.0494	1/4	1/4	1/4	1/4	0.5517	1/4	1/4
$c = 10.8460 \text{ \AA}$	0.335	0.582	0.27	0	1/2	0.7441	0.0781	0.0150	0.2167	0.7440	0.0522	0.6215	0.3195	0.4729	0.3838
	\leftrightarrow	\leftrightarrow	\leftrightarrow	\leftrightarrow	\leftrightarrow	\leftrightarrow	\leftrightarrow	\leftrightarrow	\leftrightarrow	\leftrightarrow	\leftrightarrow	\leftrightarrow	\leftrightarrow	\leftrightarrow	\leftrightarrow
$\square_2\text{Mg}_{1-x}\text{Fe}_x\text{Al}_3[\text{BO}_3][\text{SiO}_4]\text{O}_2$	Mg1	Al3	Al1	Al2	B	Si	O6	O1	O3	O7	O5	O2	O4	O5	O2
<i>Pmma</i> (no. 62)	4c	4c	4a	4b	4c	4c	8d	4c	Vacant	8d	4c	4c	4c	8d	4c
$a = 10.990 \text{ \AA}$	0.2812	0.0522	0	0	0.0003	0.2367	0.1703	0.2119	0.3789	0.4964	-0.0019	0.0992	0.4782	0.0992	0.4782
$b = 5.750 \text{ \AA}$	1/4	1/4	0	0	1/4	1/4	0.0239	1/4	1/4	1/4	1/4	1/4	1/4	0.5462	1/4
$c = 10.34 \text{ \AA}$	0.4067	0.2738	0	1/2	0.7492	0.0661	0.0077	0.2240	0.0263	0.6217	0.3196	0.4540	0.3813	0.4540	0.3813
	\leftrightarrow	\leftrightarrow	\leftrightarrow	\leftrightarrow	\leftrightarrow	\leftrightarrow	\leftrightarrow	\leftrightarrow	\leftrightarrow	\leftrightarrow	\leftrightarrow	\leftrightarrow	\leftrightarrow	\leftrightarrow	\leftrightarrow

Figure S4. Comparison of the atomic positions in $\text{Li}_2\text{Ni}[\text{PO}_4]\text{F}$ and $\text{Mg}_{1-x}\text{Fe}_x\text{Al}_3[\text{BO}_3][\text{SiO}_4]\text{O}_2$ structures.

$\text{Li}_2\text{Ni}[\text{PO}_4]\text{F}$ subcell <i>Pmma</i> (no. 62) $a_1 = 10.4730 \text{ \AA}$ $b_1 = 6.2887 \text{ \AA}$ $c_1 = 10.8460 \text{ \AA}$	Li1 8d 0.240 0.012 0.335	Li2 4c 0.271 1/4 0.582	Li3 4c 0.027 1/4 0.276	Ni1 4a 0 0 0	Ni2 4b 0 0 1/2	P1 4c 0.0236 1/4 0.7441	P2 4c 0.2432 1/4 0.0781	O1 8d 0.1891 0.0494 0.0150	O2 4c 0.2184 1/4 0.2167	O3 4c 0.1694 1/4 0.7440	O4 4c 0.3890 1/4 0.0522	O5 4c 0.4739 1/4 0.6215	O6 8d 0.0320 0.5517 0.3195	F1 4c 0.1272 1/4 0.4729	F2 4c 0.4503 1/4 0.3838		
	Symmetry reduction I_2																
$\text{Li}_5\text{Ni}[\text{PO}_4]\text{F}$ supercell $P1\ 2_1/c1$ (no. 14) $a_2 = 6.2887 \text{ \AA}$ $b_2 = 10.8460 \text{ \AA}$ $c_2 = 10.4730 \text{ \AA}$ $\beta = 90.00^\circ$	Li1_1 4e 0.488 0.335 0.26	Li1_2 4e 0.012 0.25 0.335	Li2 4e 0.25 0.582 0.229	Ni1_1 2d 1/2 0 1/2	Ni1_2 2b 0 0 0	Ni2_1 2a 0 0 0	Ni2_2 2a 0 0 0	O1_1 4e 0.4506 0.0150 0.3109	O1_2 4e 0.0494 0.0150 0.3109	O2 4e 0.25 0.2167 0.2816	O3 4e 0.75 0.2440 0.1694	O4 4e 0.25 0.0522 0.1110	O5 4e 0.25 0.6215 0.0261	O6_1 4e 0.5517 0.3195 0.4680	O6_2 4e 0.5517 0.3195 0.4680	F1 4e 0.25 0.4729 0.3728	F2 4e 0.25 0.3838 0.0497
	Symmetry reduction I_2																
$\text{Li}_5\text{V}[\text{PO}_4]_2\text{F}_2$ $P1\ 2_1/c1$ (no. 14) $a = 6.3589 \text{ \AA}$ $b = 10.7795 \text{ \AA}$ $c = 10.3836 \text{ \AA}$ $b = 90.02^\circ$	Li5 4e 0.5070 0.3352 0.2687	Li6 4e 0.0323 0.3357 0.2472	Li3 4e 0.2592 0.5834 0.2285	Li4 4e 0.2552 0.2763 0.4750	Li2 2c 1/2 0 1/2	Li1 2a 0 0 0	Vi 2a 0 0 0	O5 4e 0.4541 0.0134 0.3044	O8 4e 0.06013 0.01826 0.31701	O7 4e 0.26050 0.21791 0.28313	O4 4e 0.75630 0.24439 0.17161	O6 4e 0.23592 0.05587 0.10923	O1 4e 0.23725 0.61931 0.02574	O2 4e 0.55243 0.82422 0.46866	O3 4e 0.55243 0.47144 0.46866	F1 4e 0.22356 0.47144 0.36779	F2 4e 0.21151 0.37695 0.05764
	Symmetry reduction I_2																
$\text{Li}_5\text{Cr}[\text{PO}_4]_2\text{F}_2$ $P1\ 2_1/c1$ (no. 14) $a = 6.3135 \text{ \AA}$ $b = 10.7731 \text{ \AA}$ $c = 10.4050 \text{ \AA}$ $b = 89.91^\circ$	Li5 4e 0.479 0.330 0.2766	Li6 4e 0.021 0.323 0.222	Li3 4e 0.272 0.5913 0.2391	Li4 4e 0.276 0.2754 0.4746	Li2 2c 1/2 0 1/2	Li1 2a 0 0 0	Cr1 2a 0 0 0	O5 4e 0.4610 0.0112 0.3052	O8 4e 0.0624 0.0217 0.3154	O7 4e 0.2528 0.2242 0.2799	O4 4e 0.7394 0.2409 0.1799	O6 4e 0.2533 0.0553 0.1142	O1 4e 0.2511 0.6234 0.0254	O2 4e 0.5408 0.8209 0.4646	O3 4e 0.5408 0.3169 0.4646	F1 4e 0.2276 0.4742 0.3720	F2 4e 0.2134 0.3781 0.0566

Figure S5. Group-subgroup scheme in the Bärnighausen formalism [31, 32] for the structure of $\text{Li}_2\text{Ni}[\text{PO}_4]\text{F}$ and comparison with $\text{Li}_5M(\text{PO}_4)_2\text{F}_2$ ($M = \text{V}$ and Cr) structures. The indices of the *translationengleiche* (t) transition, as well as the unit cell and origin shift transformations are given.

3.3.3. Effect of the Li/Na ratio on the compounds with the $\text{Li}_2\text{Ni}[\text{PO}_4]\text{F}$ -type structure

When the lithium is replaced by sodium in $\text{Li}_2\text{Ni}[\text{PO}_4]\text{F}$, one would expect an increase of the cell parameters due to the large difference between the ionic radii of Li^+ and Na^+ . However, we observed that only the a and c cell parameters increased, whereas b decreased. This phenomenon has been also observed in the cobalt and iron $\text{Li}_{2-x}\text{Na}_x\text{M}[\text{PO}_4]\text{F}$ -5 systems (see the table in Fig. S6[†]). In order to explain the origin of this common behavior, projection views of the $\text{Ni}_2\text{O}_3\text{F}$ infinite chains in $\text{Li}_2\text{Ni}[\text{PO}_4]\text{F}$ and $\text{Li}_{1.3}\text{Na}_{0.7}\text{Ni}[\text{PO}_4]\text{F}$ are depicted on Fig. S6b, c[†], respectively. One can see clearly a significant tilt of the octahedra forming the $\text{Ni}_2\text{O}_3\text{F}$ infinite chains, when the lithium is partially replaced by sodium. The directions of the tilts are represented by green arrows on Fig. S6b[†]. As a consequence of these tilts, we observe an increase of the $\alpha_{\text{O}_4\text{-F}_1\text{-O}_4}$ angle from 148.84 to 160.37 °, a decrease of the $d_{\text{O}_6\text{-O}_6\text{max}}$ distance from 3.795 to 10 3.693 Å, and an increase of the $d_{\text{O}_6\text{-O}_6\text{min}}$ distance from 2.494 to 2.526 Å. This flattening of the $\alpha_{\text{O}_4\text{-F}_1\text{-O}_4}$ angle should induce an increase of the $d_{\text{Ni-Ni}}$ distance and the cell parameter b , since $b = 2 \times d_{\text{Ni-Ni}}$. This is in contradiction with experimental results which shows a decrease of cell parameter b . A more careful examination of the interatomic distances shows a decrease of the $d_{\text{O}_4\text{-F}_1\text{max}}$ from 3.264 to 3.156 Å and an increase of $d_{\text{O}_4\text{-F}_1\text{min}}$ from 2.509 to 2.654 Å. It is therefore concluded that when lithium is replaced by sodium atoms, the $\text{Ni}_2\text{O}_3\text{F}$ infinite chains are first compressed along the b -axis 15 ($d_{\text{O}_4\text{-F}_1\text{max}}$, $d_{\text{Ni-Ni}}$, and b decrease) inducing some strains, which could be reduced by a relaxation along [100] ($d_{\text{O}_4\text{-F}_1\text{min}}$ and a increase) and a tilt of the $\text{Ni}_2\text{O}_4\text{F}_2$ octahedra along [010] ($\alpha_{\text{O}_4\text{-F}_1\text{-O}_4}$ and $d_{\text{O}_6\text{-O}_6\text{min}}$ increase, whereas $d_{\text{O}_6\text{-O}_6\text{max}}$ decreases). It is worth to mention that the $\alpha_{\text{O}_4\text{-F}_1\text{-O}_4}$ angle is flexible and may reach 180 ° when the sodium content is increased. However, since O6-O6 corresponds to the edge of the PO_4 tetrahedra, the increase of $d_{\text{O}_6\text{-O}_6\text{min}}$ distance is limited. This restrains the increase of the $\alpha_{\text{O}_4\text{-F}_1\text{-O}_4}$ angle and induces a structural transition to a layered $\text{LiNaNi}[\text{PO}_4]\text{F}$ structure when a 20 critical $d_{\text{O}_6\text{-O}_6\text{min}}$ distance is reached.¹¹ Similar to $\text{Ni}_2\text{O}_3\text{F}$, the $\text{Ni}_1\text{O}_3\text{F}$ infinite chains are compressed along [010] ($d_{\text{O}_5\text{-F}_2\text{max}}$, $d_{\text{Ni-Ni}}$, and b decrease) however, the $\beta_{\text{O}_5\text{-F}_2\text{-O}_5}$ angle is less flattened than $\alpha_{\text{O}_4\text{-F}_1\text{-O}_4}$ (see table in Fig. S7[†]). The flattening of the $\alpha_{\text{O}_4\text{-F}_1\text{-O}_4}$ angle affects strongly the coordination sphere of the Li3 atom (Fig. S6a[†]), whereas the flattening of the $\beta_{\text{O}_5\text{-F}_2\text{-O}_5}$ angle affects little the coordination sphere of the Li2 atom (Fig. S7a[†]). In the cobalt, iron and magnesium $\text{Li}_{2-x}\text{Na}_x\text{M}[\text{PO}_4]\text{F}$ -systems, the same behaviors as in the nickel-system are observed, when Na replaces Li (see the table in 25 Fig. S6, 7[†]).

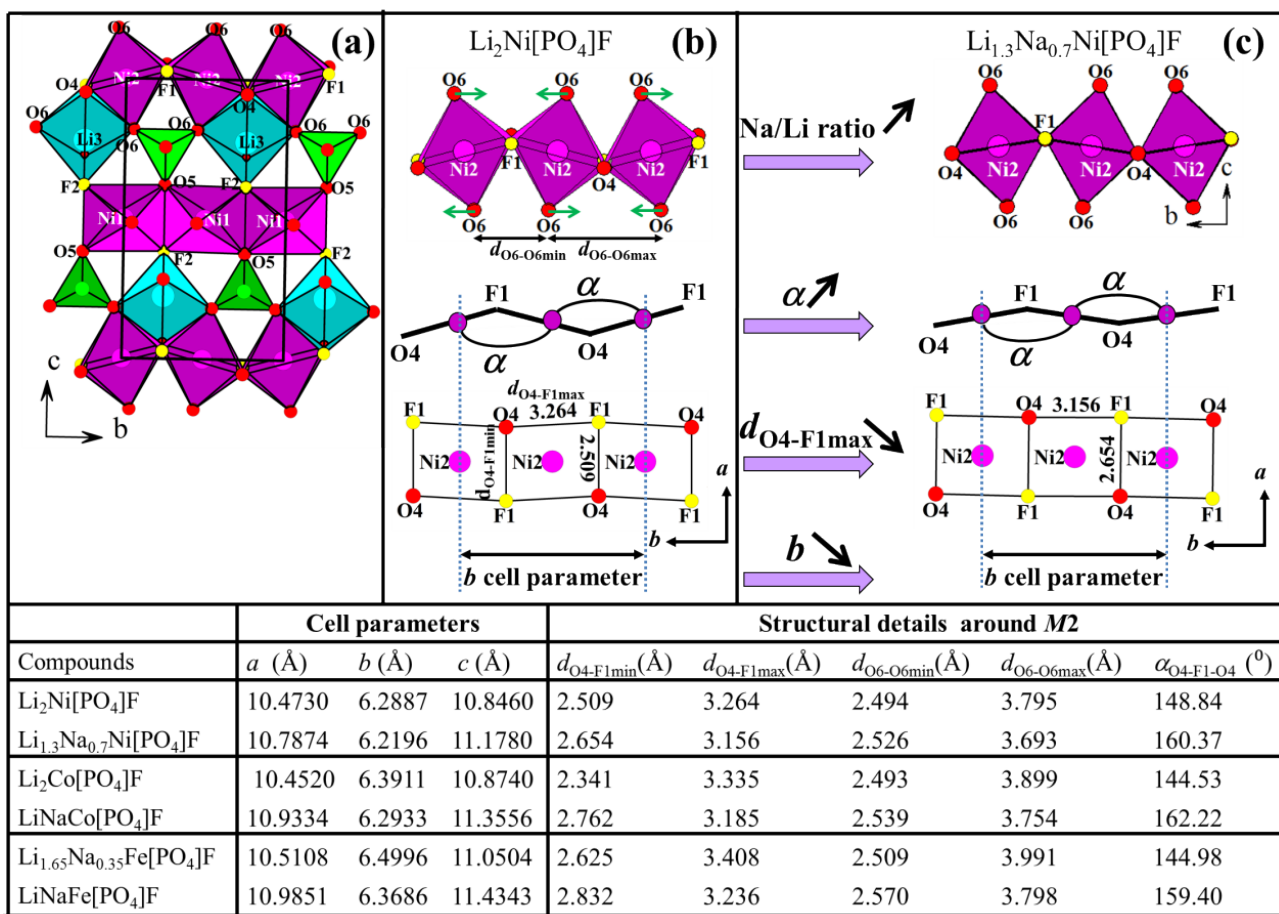


Figure S6. Projection view along [100] of the structure of $\text{Li}_2\text{Ni}[\text{PO}_4]\text{F}$ (a), and views of the infinite chains $\text{Ni}_2\text{O}_3\text{F}$, in $\text{Li}_2\text{Ni}[\text{PO}_4]\text{F}$ (b) and $\text{Li}_{1.3}\text{Na}_{0.7}\text{Ni}[\text{PO}_4]\text{F}$ (c). Crystallographic details about the compounds with $\text{Li}_2\text{Ni}[\text{PO}_4]\text{F}$ -type structure are reported in the table.

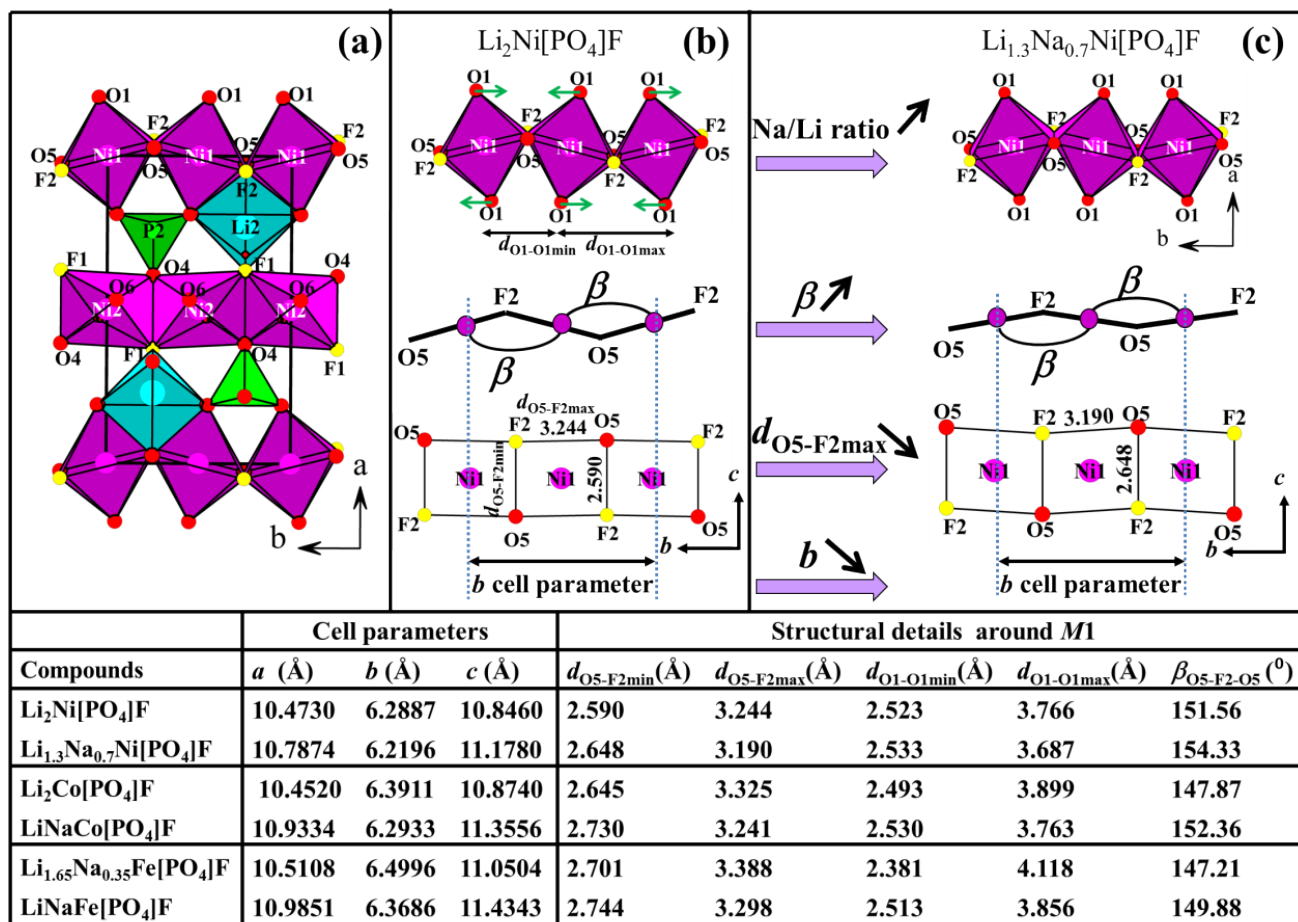


Figure S7. Projection view along [001] of the structure of $\text{Li}_2\text{Ni}[\text{PO}_4]\text{F}$ (a), and views of the infinite chains $\text{Ni}_1\text{O}_3\text{F}$, in $\text{Li}_2\text{Ni}[\text{PO}_4]\text{F}$ (b) and $\text{Li}_{1.3}\text{Na}_{0.7}\text{Ni}[\text{PO}_4]\text{F}$ (c). Crystallographic details about the compounds with $\text{Li}_2\text{Ni}[\text{PO}_4]\text{F}$ -type structure are reported in the table.

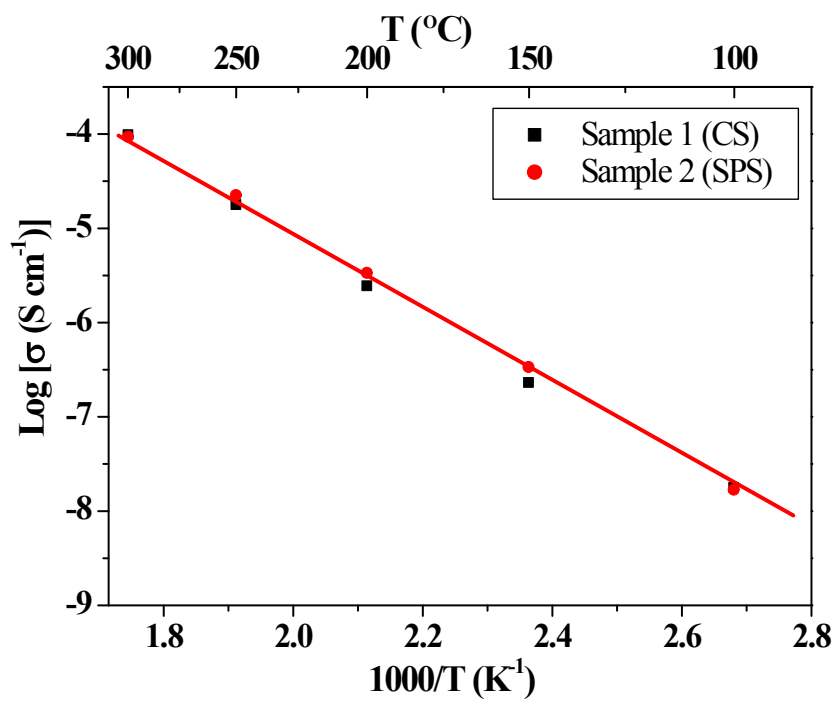


Figure S8. Arrhenius plot of the ionic conductivity σ of $\text{Li}_9\text{Mg}_3[\text{PO}_4]_4\text{F}_3\Box_1$, in air. Closed squares and open circles show samples of conventional and SPS sintering, respectively.

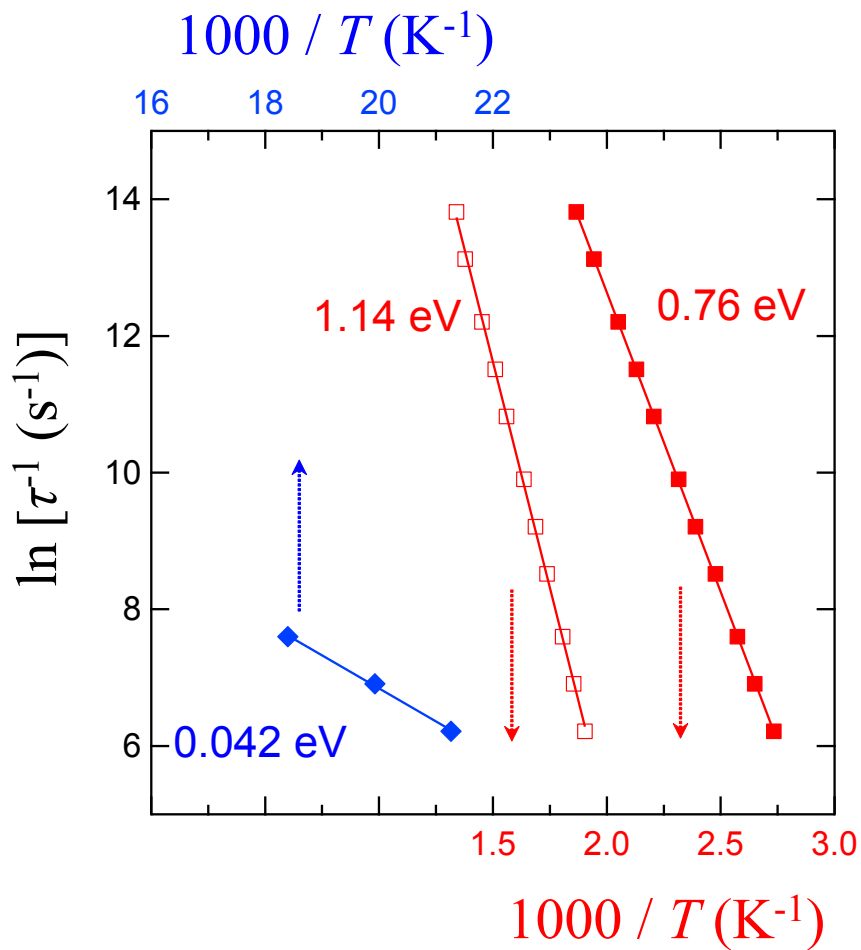


Figure S9. Arrhenius plots of the relaxation time τ^{-1} of $\text{Li}_9\text{Mg}_3[\text{PO}_4]_4\text{F}_3\Box_1$. Red closed and open squares show motions of lithium ion and anion, *e.g.* oxide and/or fluoride ion, respectively. Blue closed diamond is conserved with a mode of defective origin.³⁶

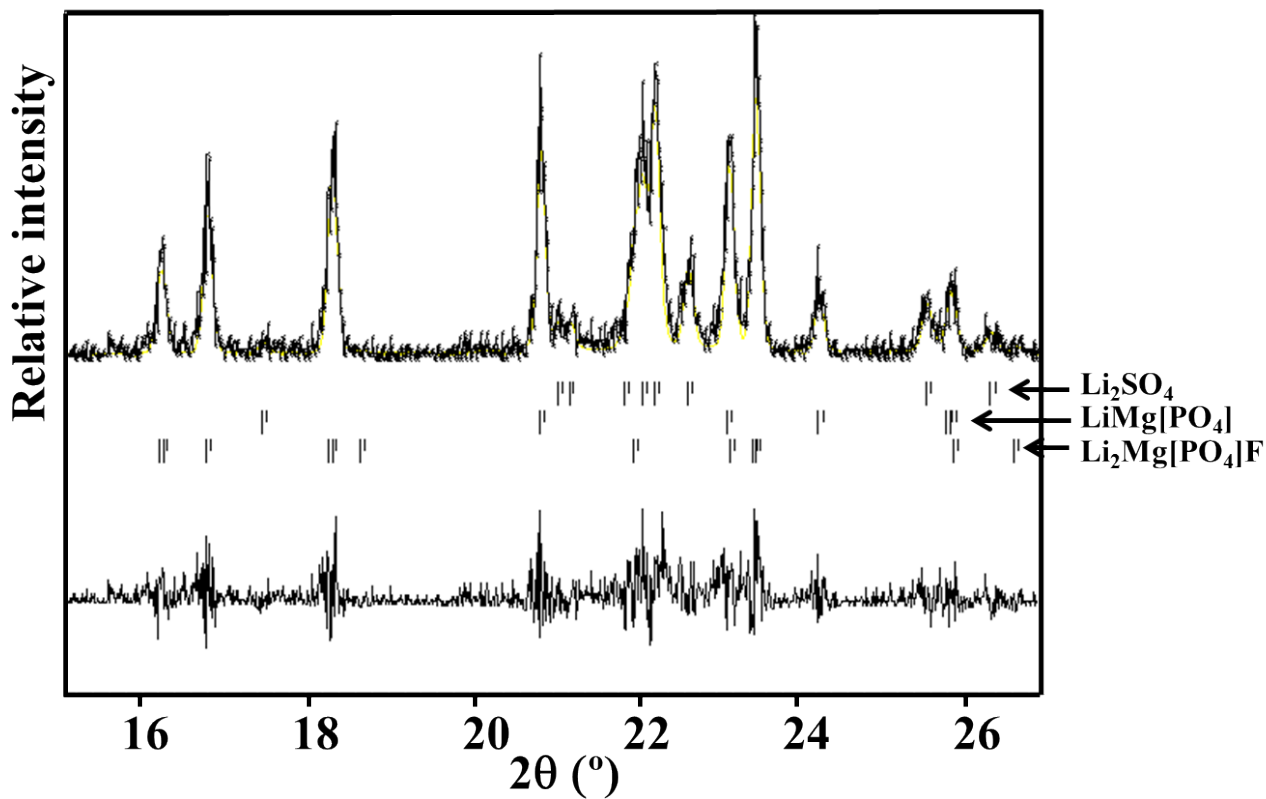


Figure S10. Observed, calculated and difference plots for the XRPD (Cu- $K\alpha$) radiation) profile refinement of the composite $\text{Li}_6\text{Mg}_4[\text{PO}_4]_3[\text{SO}_4]\text{F}_3$ material. The three phases Li_2SO_4 , $\text{LiMg}[\text{PO}_4]$ and $\text{Li}_2\text{Mg}[\text{PO}_4]\text{F}$ clearly coexist.

Table S1. Anisotropic ADPs (\AA^2) for $\text{Li}_2\text{Mg}[\text{PO}_4]\text{F}$ and $\text{Li}_9\text{Mg}_3[\text{PO}_4]_4\text{F}_3$. The anisotropic ADPfactor exponent takes the form: $-2\pi^2[(ha^*)^2U_{11}+\dots+2hka^*b^*U_{12}]$.

Atom	U_{11}	U_{22}	U_{33}	U_{12}	U_{13}	U_{23}
$\text{Li}_2\text{Mg}[\text{PO}_4]\text{F}$						
Li1	0.0382(15)	0.0345(18)	0.0253(14)	0.0087(10)	0.0047(9)	0.0079(10)
Li2	0.0143(13)	0.0137(14)	0.0141(13)	0	0.0017(9)	0
Li3/Mg3	0.0266(13)	0.0043(9)	0.0145(9)	0	-0.0023(8)	0
Mg1	0.0093(3)	0.0100(3)	0.0085(3)	-0.00051(19)	-0.00085(15)	0.00112(15)
Mg22/Li22	0.0088(3)	0.0081(3)	0.0043(3)	0.00049(19)	0.00032(15)	-0.00042(15)
P1	0.0110(2)	0.0091(2)	0.0055(2)	0	0.00110(11)	0
P2	0.0067(2)	0.0087(2)	0.0080(2)	0	0.00035(11)	0
O1	0.0096(4)	0.0102(3)	0.0166(4)	-0.0013(3)	-0.0020(2)	-0.0014(3)
O2	0.0168(6)	0.0180(5)	0.0090(5)	0	0.0023(4)	0
O3	0.0113(6)	0.0262(6)	0.0131(5)	0	0.0022(4)	0
O4	0.0081(5)	0.0106(4)	0.0171(5)	0	0.0028(4)	0
O5	0.0134(5)	0.0105(5)	0.0066(4)	0	-0.0001(3)	0
O6	0.0224(4)	0.0097(4)	0.0082(3)	0.0019(3)	0.0007(3)	0.0011(3)
F1	0.0104(5)	0.0138(4)	0.0182(4)	0	-0.0025(3)	0
F2	0.0173(5)	0.0146(4)	0.0107(4)	0	0.0001(3)	0
$\text{Li}_9\text{Mg}_3[\text{PO}_4]_4\text{F}_3$						
Li1	0.013(3)	0.021(3)	0.021(3)	0.0043(17)	0.002(2)	0.007(2)
Li2	0.035(3)	0.021(2)	0.017(3)	0.008(3)	0.003(3)	-0.0047(19)
Li3	0.0028(17)	0.003(2)	0.0064(17)	-0.0010(13)	0.0020(18)	0.002(2)
Mg1	0.0090(3)	0.0082(4)	0.0102(4)	0.0044(3)	-0.0001(5)	0.0000(4)
P1	0.0085(3)	0.0067(3)	0.0086(3)	0.00422(19)	0.0001(3)	0.0003(4)
P2	0.0073(3)	0.0073(3)	0.0085(6)	0.00366(15)	0	0
O1	0.0110(10)	0.0104(9)	0.0120(8)	0.0069(6)	0.0006(8)	0.0015(8)
O2	0.0093(8)	0.0130(9)	0.0165(9)	0.0055(9)	0.0009(7)	-0.0008(12)
O3	0.0161(10)	0.0106(9)	0.0116(9)	0.0082(8)	-0.0010(7)	-0.0014(7)
O4	0.0172(10)	0.0098(9)	0.0111(11)	0.0068(8)	-0.0035(8)	-0.0032(7)
O5	0.0138(8)	0.0109(8)	0.0103(8)	0.0063(7)	0.0020(7)	0.0009(9)
O6	0.0141(9)	0.0141(9)	0.0117(14)	0.0070(5)	0	0
F1	0.0115(8)	0.0111(6)	0.0132(6)	0.0036(6)	0.0029(7)	0.0007(5)

Table S2. Comparison of the crystallographic data of $\text{Li}_9\text{Mg}_3[\text{PO}_4]_4\text{F}_3\Box_1$ and $\text{Na}_8\text{Mn}_4[\text{PO}_4]_4\text{F}_4$ after lowering the symmetries from $P6_3$ and $P2_1/c$ to $P2_1$, respectively. The main differences are highlighted in red.

$\text{Li}_9\text{Mg}_3[\text{PO}_4]_4\text{F}_3\Box_1$ [Space group : $P2_1$ (No. 4)] $a = 12.6159(6) \text{ \AA}$, $b = 5.0082(4) \text{ \AA}$, $c = 12.6159(6) \text{ \AA}$, $\beta = 120^\circ$, $V = 690.32(7) \text{ \AA}^3$, $Z = 2$				$\text{Na}_8\text{Mn}_4[\text{PO}_4]_4\text{F}_4$ [Space group : $P2_1$ (No. 4)] $a = 13.6830 \text{ \AA}$, $b = 5.3170 \text{ \AA}$, $c = 13.7683 \text{ \AA}$ $\beta = 120.04^\circ$, $V = 867.13 \text{ \AA}^3$, $Z = 2$			
Atom	x	y	z	Atom	x	y	z
Li1a	0.91596	0.34609	0.08346	Na1_2	0.92016	0.26170	0.08350
Li1b	0.83250	0.84609	0.91596	Na4_2	0.83455	0.73700	0.92191
Li1c	0.91654	0.34609	0.83250	Mn2_2	0.92356	0.22901	0.85041
Li2a	0.82524	0.79962	0.42936	Na4_1	0.83455	0.76300	0.42191
Li2b	0.60412	0.79962	0.17476	Na2_2	0.58023	0.75620	0.16325
Li2c	0.57064	0.79962	0.39588	Mn1_1	0.57610	0.77224	0.42666
Li3a	0.91379	0.27109	0.57909	Na1_1	0.92016	0.23830	0.58350
Li3b	0.66530	0.27109	0.08621	Na3_2	0.66608	0.25860	0.08680
Li3c	0.42091	0.27109	0.33470	Na2_1	0.41977	0.24380	0.33675
Mg1a	0.93254	0.26874	0.35849	Mn2_1	0.92356	0.27099	0.35041
Mg1b	0.42594	0.26874	0.06745	Mn1_2	0.42390	0.22776	0.07334
Mg1c	0.64152	0.26874	0.57406	Na3_1	0.66608	0.24140	0.58680
P1b	0.84677	0.75424	0.16576	P2_2	0.83782	0.78350	0.17335
O2b	0.90816	0.75313	0.08608	O5_2	0.90370	0.70190	0.11520
O5b	0.83408	0.45809	0.19409	O4_1	0.85110	0.07170	0.19420
O4b	0.92631	0.90619	0.28440	O1_1	0.88340	0.64650	0.28620
O3b	0.71920	0.88192	0.09711	O6_2	0.71190	0.72140	0.09830
P2	0.33333	0.79544	0.66667	P1_1	0.33795	0.78560	0.66529
O1c	0.59815	0.18600	0.20247	O2_2	0.59730	0.21450	0.21010
O1b	0.79753	0.18600	0.39568	O8_1	0.78750	0.22010	0.38520
O1a	0.60432	0.18600	0.40185	O3_1	0.61400	0.14660	0.39900
O6	0.66667	0.60217	0.33333	O7_1	0.65150	0.57390	0.34630
P1a	0.83424	0.75424	0.68101	P2_1	0.83782	0.71650	0.67335
O3a	0.90289	0.88192	0.62208	O5_1	0.90370	0.79810	0.61520
O5a	0.80591	0.45809	0.63999	O4_2	0.85110	0.42830	0.69420
O2a	0.91392	0.75313	0.82209	O1_2	0.88340	0.85350	0.78620
O4a	0.71560	0.90619	0.64191	O6_1	0.88340	0.85350	0.78620
P1c	0.68101	0.25424	0.84677	P1_2	0.66205	0.21440	0.83471
O3c	0.62208	0.38192	0.71920	O2_1	0.59730	0.28550	0.71010
O4c	0.64191	0.40619	0.92631	O3_2	0.61400	0.35340	0.89900
O2c	0.82209	0.25313	0.90816	O8_2	0.78750	0.27990	0.88520
O5c	0.63999	-0.04191	0.83408	O7_2	0.65150	-0.07390	0.84630
F1a	0.03892	0.07408	0.52264	F1_1	0.00030	0.00040	0.48680
F1b	0.51628	0.57408	0.03892	F2_2	0.49270	0.50160	0.00860
F1c	0.47736	0.07408	0.51628	F2_1	0.49270	-0.00160	0.50860
Vacant	-	-	-	F1_2	0.00030	0.49960	0.98680